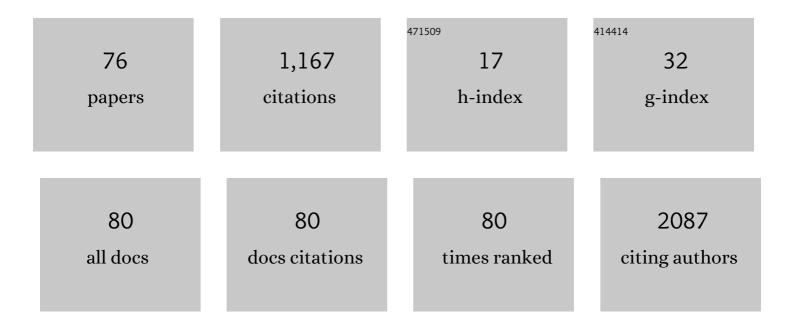
List of Publications by Year in descending order

Source: https://exaly.com/author-pdf/8675948/publications.pdf Version: 2024-02-01



#	Article	IF	CITATIONS
1	Magnetic Properties of Single-Crystalline CoSi Nanowires. Nano Letters, 2007, 7, 1240-1245.	9.1	132
2	Cobalt nanofibers encapsulated in a graphite shell by an electrospinning process. Journal of Materials Chemistry, 2009, 19, 7371.	6.7	120
3	Long-range chiral exchange interaction in synthetic antiferromagnets. Nature Materials, 2019, 18, 703-708.	27.5	83
4	Thermoelectric properties of Mn-doped Mg–Sb single crystals. Journal of Materials Chemistry A, 2014, 2, 12311-12316.	10.3	78
5	Spin-orbit torque in a bulk perpendicular magnetic anisotropy Pd/FePd/MgO system. Scientific Reports, 2014, 4, 6548.	3.3	59
6	In situ fabrication of cobalt-doped SrFe2As2 thin films by using pulsed laser deposition with excimer laser. Applied Physics Letters, 2009, 95, 062507.	3.3	40
7	Magnetic Transition to Antiferromagnetic Phase in Gadolinium Substituted Topological Insulator Bi2Te3. Scientific Reports, 2015, 5, 10309.	3.3	37
8	Room Temperature Ferromagnetism in Single-Crystalline Fe ₅ Si ₃ Nanowires. Journal of Physical Chemistry C, 2009, 113, 6902-6905.	3.1	36
9	Effects of sputtering Ar gas pressure in the exchange stiffness constant of Co40Fe40B20 thin films. Journal of Magnetism and Magnetic Materials, 2013, 339, 36-39.	2.3	32
10	Studying the reduction of graphene oxide with magnetic measurements. Carbon, 2019, 142, 373-378.	10.3	32
11	Single-Crystalline Ferromagnetic Fe1-xCoxSi Nanowires. Journal of Physical Chemistry C, 2008, 112, 4748-4752.	3.1	31
12	Fluctuation conductivity of single-crystalline BaFe1.8Co0.2As2 in the critical region. Journal of Applied Physics, 2010, 108, .	2.5	30
13	Role of top and bottom interfaces of a Pt/Co/AlOx system in Dzyaloshinskii-Moriya interaction, interface perpendicular magnetic anisotropy, and magneto-optical Kerr effect. AlP Advances, 2017, 7, .	1.3	26
14	Polarity-tunable magnetic tunnel junctions based on ferromagnetism at oxide heterointerfaces. Nature Communications, 2015, 6, 8035.	12.8	24
15	Facile synthesis of fully ordered L10-FePt nanoparticles with controlled Pt-shell thicknesses for electrocatalysis. Nano Research, 2017, 10, 2866-2880.	10.4	24
16	Magnetic properties of Mn and Co doped PbPdO2. Journal of Applied Physics, 2011, 109, .	2.5	21
17	In-Depth Structural Characterization of 1T-VSe ₂ Single Crystals Grown by Chemical Vapor Transport. Crystal Growth and Design, 2020, 20, 2860-2865.	3.0	21
18	Observation of Restored Topological Surface States in Magnetically Doped Topological Insulator. Scientific Reports, 2019, 9, 1331.	3.3	17

#	Article	IF	CITATIONS
19	Dependence of the switching current density on the junction sizes in spin transfer torque. Journal of Applied Physics, 2013, 113, .	2.5	16
20	Structural and magnetic properties of highly Fe-doped ZnO nanoparticles synthesized by one-step solution plasma process. Journal of Alloys and Compounds, 2021, 853, 157153.	5.5	16
21	Ferromagnetism in undoped ZnO nanostructures synthesized by solution plasma process. Current Applied Physics, 2017, 17, 181-185.	2.4	14
22	Ferromagnetism in ZnCoO due to Hydrogen-Mediated Co–H–Co Complexes: How to Avoid the Formation of Co Metal Clusters?. Journal of Physical Chemistry C, 2012, 116, 12196-12202.	3.1	13
23	Thermoelectric Properties of a Single Crystalline Ag ₂ Te Nanowire. Journal of Nanomaterials, 2017, 2017, 1-5.	2.7	13
24	Structural, magnetic, and electrical properties of collinear antiferromagnetic heteroepitaxy cubic Mn3Ga thin films. Applied Physics Letters, 2019, 115, .	3.3	13
25	Perpendicular magnetic anisotropy properties of tetragonal Mn 3 Ga films under various deposition conditions. Current Applied Physics, 2016, 16, 63-67.	2.4	12
26	Facile solid-state synthesis of oxidation-resistant metal nanoparticles at ambient conditions. Solid State Sciences, 2018, 79, 38-47.	3.2	12
27	Spin wave quantization in continuous film with stripe domains. Journal of Applied Physics, 2009, 105, 07D544.	2.5	10
28	Fabrication and temperature-dependent magnetic properties of one-dimensional embedded nickel segment in gold nanowires. Journal of Alloys and Compounds, 2012, 541, 483-487.	5.5	10
29	Effect of oxidizing the ferromagnetic electrode in magnetic tunnel junctions on tunneling magnetoresistance. Applied Physics Letters, 2012, 100, 172406.	3.3	10
30	Fabrication and temperature-dependent magnetic properties of one-dimensional multilayer Au–Ni–Au–Ni–Au nanowires. Journal of Solid State Chemistry, 2014, 210, 116-120.	2.9	10
31	Exploring Highâ€Energy Liâ€I(r)on Batteries and Capacitors with Conversionâ€Type Fe ₃ O ₄ â€rGO as the Negative Electrode. ChemElectroChem, 2017, 4, 2626-2633.	3.4	10
32	Electronic properties of Gd <i>x</i> Bi2â^' <i>x</i> Se3 single crystals analyzed by Shubnikov-de Haas oscillations. Applied Physics Letters, 2018, 112, .	3.3	9
33	Time-dependent magnetization reversal in amorphous CoSiB/Pd multilayers with perpendicular magnetic anisotropy. Journal of Applied Physics, 2013, 113, .	2.5	7
34	Figure of merit of <scp>X</scp> â€ŧype hexaferrite (<scp>B</scp> a ₂ <scp>C</scp> o ₂ <scp>F</scp> e ₂₈ <scp>O</scp> for mobile antenna applications. Microwave and Optical Technology Letters, 2018, 60, 795-799.	ł6⊯asub>)	7
35	Gd doping effect in p-type Bi2Te3 single crystals. AIP Advances, 2018, 8, 101319.	1.3	7
36	Current- and Field-Driven Domain Wall Motion in L- and C-Shaped Permalloy Nanowires With Different Wire Widths. IEEE Transactions on Magnetics, 2008, 44, 2527-2530.	2.1	6

#	Article	IF	CITATIONS
37	Stability of Magnetic Domains With Notches in Permalloy Nanowires. IEEE Transactions on Magnetics, 2009, 45, 2481-2484.	2.1	6
38	Electronic structures of MnB soft magnet. AIP Advances, 2016, 6, .	1.3	6
39	Skyrmion Phase in MnSi Thin Films Grown on Sapphire by a Conventional Sputtering. Nanoscale Research Letters, 2021, 16, 7.	5.7	6
40	Magnetic and structural phase transitions by annealing in tetragonal and cubic Mn3Ga thin films. Journal of Alloys and Compounds, 2021, 869, 159346.	5.5	6
41	Orbit topology analyzed from π phase shift of magnetic quantum oscillations in three-dimensional Dirac semimetal. Proceedings of the National Academy of Sciences of the United States of America, 2021, 118, .	7.1	6
42	Correlation between the magnetic and thermoelectric properties in Mg2â^'Mn Si. Journal of Alloys and Compounds, 2017, 690, 51-56.	5.5	5
43	Gradual phase transition from ferromagnetic tetragonal to antiferromagnetic cubic states in Mn Ga (1.80 â‰ष â‰ष्3.03) thin films. Journal of Alloys and Compounds, 2019, 810, 151988.	5.5	5
44	Highly Reduced Saturation Magnetization in Epitaxially Grown Ferrimagnetic Heusler Thin Films. ACS Omega, 2019, 4, 16578-16584.	3.5	5
45	Current induced chiral domain wall motion in Culr/CoFeB/MgO thin films with strong higher order spin–orbit torques. Applied Physics Letters, 2020, 116, .	3.3	5
46	Proximityâ€Induced Magnetism Enhancement Emerged in Chiral Magnet MnSi/Topological Insulator Bi 2 Se 3 Bilayer. Advanced Quantum Technologies, 2021, 4, 2000124.	3.9	5
47	Structural and Magnetic Properties of Amorphous and Nanocrystalline CoFeSiB Thin Films. IEEE Nanotechnology Magazine, 2008, 7, 409-411.	2.0	4
48	Magnetic instability of MgB2 thin film triggered by the various sweeping rates of an applied magnetic field. Journal of Applied Physics, 2010, 107, 013902.	2.5	4
49	Saw-tooth pattern from flux jumps observed by high resolution M-H curves in MgB2 thin films. Journal of Applied Physics, 2010, 108, .	2.5	4
50	Emergence of non-Fermi-liquid type Weyl metals driven by doped magnetic impurities in spin-orbit coupled semiconductors. Physical Review B, 2018, 98, .	3.2	4
51	Effect of antiferromagnetic order on topological electronic structure in Eu-substituted Bi2Se3 single crystals. APL Materials, 2020, 8, 111108.	5.1	4
52	Rare-earth-doped Bi ₂ <i>X</i> ₃ (<i>X</i> = Se, Te) as candidates for magnetic topological insulators. Philosophical Magazine, 2020, 100, 1258-1267.	1.6	4
53	Suppressing antiferromagnetic coupling in rare-earth free ferromagnetic MnBi-Cu permanent magnet. Journal of Applied Physics, 2021, 129, .	2.5	4
54	Possible permanent Dirac- to Weyl-semimetal phase transition by ion implantation. NPG Asia Materials, 2022, 14, .	7.9	4

#	Article	IF	CITATIONS
55	Single-crystal like mesoporous ZnO:Mn2+ nanorings of high optoelectronic quality formed by self-assembly of nanoparticles in an ultrasonic hydrolysis process. Nanoscale, 2011, 3, 4962.	5.6	3
56	Giant magnetic flux jumps in single crystals of Ba0.6K0.4Fe2As2. Applied Physics Letters, 2011, 98, .	3.3	3
57	Role of non-collinear polarizer layer in spin transfer torque switching processes. Journal of Applied Physics, 2013, 114, .	2.5	3
58	Confined condensation synthesis and magnetic properties of layered copper hydroxide frameworks. Dalton Transactions, 2017, 46, 3363-3368.	3.3	3
59	Angle-resolved photoemission spectroscopy study of magnetic topological insulator candidates of Ce-doped Bi2–xCexSe3. Applied Physics Letters, 2019, 115, 072404.	3.3	3
60	Photoemission and soft X-ray absorption spectroscopy study of Gd-substituted thermoelectric and topological Bi2Te3. Journal of Electron Spectroscopy and Related Phenomena, 2019, 230, 21-25.	1.7	3
61	Signature of topological states in antiferromagnetic Sm-substituted Bi2Te3. Scientific Reports, 2020, 10, 9615.	3.3	3
62	Emergence of the topological Hall effect in a tetragonal compensated ferrimagnet Mn2.3Pd0.7Ga. NPG Asia Materials, 2021, 13, .	7.9	3
63	Hall effect and magnetoresistance of YbAl3. Physica B: Condensed Matter, 2002, 312-313, 354-355.	2.7	2
64	Concurrent magnetic and metal-insulator transitions in Eu1â^'xSmxB6 single crystals. Applied Physics Letters, 2009, 94, 042509.	3.3	2
65	Giant Magnetic Moment of Oxygen-Free CuNi Nanoparticles. Journal of Nanoscience and Nanotechnology, 2009, 9, 3201-3203.	0.9	2
66	Magnetotransport Properties and Kondo Effect Observed in a Ferromagnetic Singleâ€Crystalline Fe _{1â~²<i>x</i>} Co _{<i>x</i>} Si Nanowire. Chemistry - an Asian Journal, 2012, 7, 406-411.	3.3	2
67	The Azimuthal Dependence of Exchange Bias Effect and its Analysis by Spin Glass Model in Ni _{0.8} Fe _{0.2} /Co _x Ni _{1â^*x} O Bilayers. IEEE Access, 2021, 9, 21315-21322.	4.2	2
68	Oscillatory Interlayer Exchange Coupling in Amorphous CoSiB/Pt/CoSiB Structure. IEEE Transactions on Magnetics, 2015, 51, 1-4.	2.1	1
69	Exchange Bias Effect Determined by Anisotropic Magnetoresistance in CoxNi1â^'xO/Ni0.8Fe0.2 Bilayer System. IEEE Transactions on Magnetics, 2015, 51, 1-4.	2.1	1
70	Fine tuning of the magnetic properties in Mn3-Co Ga Heusler films near the critical regime. Journal of Alloys and Compounds, 2021, 858, 158288.	5.5	1
71	Ferromagnetism in β-Ag2Se topological semimetal. Journal of Alloys and Compounds, 2022, 891, 162025.	5.5	1
72	Impact of Dark Excitons on the Population and Relaxation Kinetics of Two-Dimensional Biexcitons in [CH3(CH2)3NH3]2Pb1–xMnxBr4 (x = 0–0.09). Journal of the American Chemical Society, 2021, 143, 19785-19793.	13.7	1

#	Article	IF	CITATIONS
73	Berry paramagnetism in the Dirac semimetal ZrTe5. Communications Physics, 2021, 4, .	5.3	1
74	Temperature Dependence of the Dielectric Response and Critical Point Energies of Bi1.85Gd0.15Te3. Journal of Nanoscience and Nanotechnology, 2018, 18, 6321-6325.	0.9	0
75	Upper Limit of Carbon Concentration in Ferromagnetic L1â,€-Ordered FePt-C for Tb/in² Data Storage Density Heat-Assisted Magnetic Recording Media. IEEE Transactions on Magnetics, 2021, 57, 1-6.	2.1	Ο
76	Functionalities enhancement by an anisotropic strain competition. Ferroelectrics, 2021, 583, 264-277.	0.6	0